Critique of Velocity/Wave-Vector PDF Modeling

by

P.R. Van Slooten
and
S.B. Pope

FDA 97-09 December 1997

1 Introduction

The velocity/wave-vector PDF method was developed for inhomogeneous turbulent flows in Van Slooten and Pope [1] where several wave vector models (WVM's) were introduced. The formulation is based on the particle representation model (PRM) of Kassinos and Reynolds [2] and provides an exact description for the rapid distortion of homogeneous turbulence (RDT). The PRM is extended to general homogeneous turbulence in Kassinos and Reynolds [3] through the interacting particle representation model (IPRM). The purpose of this report is to express the IPRM in the form of a WVM and to critique the various WVM's.

2 Model Formulations

2.1 Wave Vector Models

An exact representation of RDT is achieved by adding a unit vector, the wave vector, into the PDF formulation. Since PDF methods are typically applied via stochastic models for the behavior of a fluid particle, a stochastic system in the WVM approach requires an additional model for the wave vector, $\mathbf{e}^*$. The particle fluctuating velocity, $\mathbf{u}^*$, and wave vector evolve in RDT by ordinary differential equations,

$$du_i^* = -\frac{\partial \langle U_r \rangle}{\partial x_s} u_s^* (\delta_{ir} - 2e_i^* e_r^*) dt \tag{1}$$

and

$$de_i^* = -\frac{\partial \langle U_r \rangle}{\partial x_s} e_r^* (\delta_{is} - e_i^* e_s^*) dt, \tag{2}$$

where the Eulerian mean velocity gradient, $\partial \langle U_r \rangle / \partial x_s$, is specified for homogeneous turbulence. The details of the analysis from a PDF point of view are contained in Van Slooten and Pope [1] and are based on the development of the PRM from Kassinos and Reynolds [2].

The Reynolds stress equation is simplified in RDT by neglecting the dissipation of turbulent kinetic energy, ε, and the return-to-isotropy tensor,

$$\phi_{ij} \equiv -\frac{1}{\varepsilon} \Pi_{ij}^{(s)} + 2e_{ij}, \tag{3}$$

where $\Pi_{ij}^{(s)}$ is the slow pressure–rate-of-strain correlation and $e_{ij} \equiv \varepsilon_{ij}/(2\varepsilon) - \delta_{ij}/3$ is the normalized anisotropy of the dissipation tensor, ε_{ij}. The rapid pressure–rate-of-strain correlation is still unclosed in the Reynolds stress equation and is in RDT exactly represented by the WVM. For non-RDT homogeneous turbulence, a "decay" model is added to Eqs. (1) and (2) to model the return-to-isotropy tensor, which is the only unclosed term in the Reynolds stress anisotropy equation for decaying turbulence. The decay models are constructed independently of the RDT equations, but do alter the model for the rapid pressure–rate-of-strain correlation

through an effect on $M_{ijpq} \equiv \langle u_i^* u_j^* e_p^* e_q^* \rangle / 2k$. This tensor is contracted with the mean velocity gradient to yield the model for the rapid pressure–rate-of-strain correlation.

The general **u-e** decay model is derived from the general form of two coupled vector-valued diffusion processes by imposing four constraints on the system (Van Slooten and Pope [1]). Two constraints are deterministic and apply to every realization of system. They are:

1. $\mathbf{e}^*$ remains of unit length (by definition);

2. $\mathbf{e}^*$ and $\mathbf{u}^*$ maintain orthogonality due to the continuity equation in Fourier space.

The remaining two constraints are based on physical arguments for decaying turbulence and impose restrictions on the statistical behavior of the system. They are:

3. the PDF of velocity tends to an isotropic joint-normal distribution;

4. the evolution of the turbulent kinetic energy is known

$$\frac{dk}{dt} = -\varepsilon. \tag{4}$$

The general model is far too complex for a realistic application, but it serves as a guide to the construction and analysis of specific models that are based on assumptions into the behavior of the system.

Beyond providing an exact representation of RDT, the WVM's represent the structure dimensionality and circulicity tensors (Kassinos and Reynolds [2]) without additional assumptions

$$D_{ij} \leftrightarrow \langle e_i^* e_j^* u_s^* u_s^* \rangle \tag{5}$$

and

$$F_{ij} \leftrightarrow \epsilon_{ilm} \epsilon_{jnp} \langle e_l^* e_n^* u_m^* u_p^* \rangle, \tag{6}$$

where ϵ_{ilm} is the alternating symbol. The structure dimensionality tensor provides information on the directions of dimensional independence, and the structure circulicity tensor provides information on the large-scale vorticity field. The normalized tensors, $d_{ij} \equiv D_{ij}/(2k)$ and $f_{ij} \equiv F_{ij}/(2k)$, and the normalized anisotropies, $d_{ij}^a \equiv d_{ij} - \delta_{ij}/3$ and $f_{ij}^a \equiv f_{ij} - \delta_{ij}/3$, are available for modeling of terms like the return-to-isotropy tensor. Also available are the Reynolds stress tensor, $\langle u_i u_j \rangle$, the normalized Reynolds stress tensor, $r_{ij} \equiv \langle u_i u_j \rangle / (2k)$, and the anisotropy of the Reynolds stress tensor, $b_{ij} \equiv r_{ij} - \delta_{ij}/3$.

2.2 Isotropic Diffusion of e Model (Iso model)

The first decay model constructed in Van Slooten and Pope [1] is the isotropic diffusion of **e** model. The model assumes an isotropic diffusion or random walk of $\mathbf{e}^*$ on the unit sphere with a time scale proportional to the turbulent time scale

$$de_i^* = -\left(\frac{a_e\varepsilon}{k}\right)e_i^* dt + \left(\frac{a_e\varepsilon}{k}\right)^{1/2}\left[\delta_{il} - e_i^* e_l^*\right] dW_l, \tag{7}$$

where a_e is a model parameter and $\boldsymbol{W}(t)$ is an independent, vector-valued Wiener process. Applying the constraints of a decay model and assuming that the randomization of $\mathbf{u}^*$ relative to $\mathbf{e}^*$ is described by a simple diffusion process, the stochastic velocity equation becomes

$$\begin{aligned} du_i^* &= -\frac{1}{2}\left(\frac{\varepsilon}{k}\right)\left[1 + \frac{3}{2}a_u + a_e\right]u_i^* dt + \frac{1}{2}(a_u\varepsilon)\frac{u_i^*}{u_s^* u_s^*}dt \\ &\quad -\left(\frac{a_e\varepsilon}{k}\right)^{1/2} e_i^* u_l^* dW_l + (a_u\varepsilon)^{1/2}\left[\delta_{il} - e_i^* e_l^*\right] dW_l', \end{aligned} \tag{8}$$

where a_u is a model parameter and $\boldsymbol{W}'(t)$ is another independent, vector-valued Wiener process. The parameters $(a_e,\, a_u) = (0.3,\, 0.3)$ are specified through comparison with experimental and direct numerical simulation (DNS) data in homogeneous shear. At the Reynolds stress level, the Iso model represents the return-to-isotropy tensor as

$$\phi_{ij} = (2 + 3a_u)\, b_{ij} + 2a_e\left(b_{ij} - d_{ij}^a\right) + a_u\left[\langle e_i^* e_j^*\rangle - \left\langle\frac{u_i^* u_j^*}{u_s^* u_s^*}\right\rangle\right]. \tag{9}$$

The model is linear in the anisotropies of the Reynolds stress and structure dimensionality tensors, but contains additional tensors whose behavior has less physical meaning.

2.3 Langevin Velocity Model (Lang model)

The Langevin velocity model is constructed in Van Slooten and Pope [1] by specifying the Langevin equation with an anisotropic drift term as the model for the particle velocity,

$$\begin{aligned} du_i^* &= -\frac{1}{2}\left(\frac{\varepsilon}{k}\right)\left[1 + \frac{3}{2}a_u\right]u_i^* dt + \left(\frac{\gamma\varepsilon}{k}\right)\left[b_{ij} - b_{mn}b_{mn}\delta_{ij}\right]u_j^* dt \\ &\quad +(a_u\varepsilon)^{1/2} dW_i, \end{aligned} \tag{10}$$

where a_u and γ are model parameters. The corresponding model for the wave vector is derived by applying the decay model constraints

$$\begin{aligned} de_i^* &= -\frac{1}{2}\left(\frac{\varepsilon}{k}\right)\left[a_e + a_u\frac{k}{u_s^* u_s^*}\right]e_i^* dt - \left(\frac{\gamma\varepsilon}{k}\right)\left[\delta_{ij} - e_i^* e_j^*\right]b_{jl}e_l^* dt \\ &\quad -(a_u\varepsilon)^{1/2}\left[\frac{u_i^* e_l^*}{u_s^* u_s^*}\right]dW_l + \left(\frac{a_e\varepsilon}{k}\right)^{1/2}\left[\delta_{il} - e_i^* e_l^* - \frac{u_i^* u_l^*}{u_s^* u_s^*}\right]dW_l', \end{aligned} \tag{11}$$

where a_e is a model parameter. The motivation of the model is a representation of the return-to-isotropy tensor that is a closed general function of the Reynolds stress anisotropies

$$\phi_{ij} = \left[2 + 3a_u - 4\gamma\left(\frac{1}{3} - b_{mn}b_{mn}\right)\right] b_{ij} - 4\gamma\left(b_{il}b_{lj} - \frac{1}{3}b_{mn}b_{mn}\delta_{ij}\right). \tag{12}$$

The model parameters (a_e, a_u, γ) = (0.03, 2.1, 2.0) are set to constant values through comparisons with experimental and DNS data in a homogeneous shear flow.

2.4 Interacting Particle Representation Model (IPRM)

In the IPRM of Kassinos and Reynolds [3], the modeling of non-RDT homogeneous turbulence is viewed as an interaction between particles that results in an additional velocity gradient. The *effective* gradient is defined as the sum of the mean deformation and the particle interaction gradient. The interaction of particles is also assumed to add a rotational randomization of the velocity vector about the wave vector which is modeled by the slow rotational randomization (SRR) model. The SRR model has no effect on the energy of particles and vanishes when the circulicity tensor lies in the plane normal to the wave vector. The details of the analysis are located in Kassinos and Reynolds [3].

The decay model contained in the IPRM is expressed in the notation of the WVM as

$$de_i^* = -\left(\frac{a_e\varepsilon}{k}\right) g_{mn}e_m^* \left[\delta_{in} - e_i^*e_n^*\right] dt \tag{13}$$

and

$$\begin{aligned} du_i^* \;=\; & -\left(\frac{\varepsilon}{2k}\right) g_{mn}u_n^* \left[\delta_{im} - (2a_e{+}1)e_i^*e_m^*\right] dt - \left(\frac{a_u\varepsilon}{k}\right) \hat{\Omega}^* f_{pq}e_p^*e_q^*u_i^* dt \\ & - \left[\left(\frac{a_u\varepsilon}{k}\right) \hat{\Omega}^* f_{pq}e_p^*e_q^*u_s^*u_s^*\right]^{1/2} \epsilon_{ipq} dW_p e_q^*, \end{aligned} \tag{14}$$

where the normalized interaction gradient tensor, $\boldsymbol{g}$, and the normalized effective rotation rate, $\hat{\Omega}^*$, are defined by

$$g_{ij} \equiv \frac{r_{il}d_{lj}}{r_{pq}d_{qs}r_{sp}} = \frac{1}{4k^2}\frac{\langle u_i^*u_l^*\rangle\langle e_l^*e_j^*u_s^*u_s^*\rangle}{r_{pq}d_{qs}r_{sp}} \tag{15}$$

and

$$\hat{\Omega}^* \equiv \sqrt{g_{mn}\left(g_{mn} - g_{nm}\right)}. \tag{16}$$

The parameters (a_e, a_u) = (1.1, 4.25) are calculated from the values given in Kassinos and Reynolds [3].

The normalized interaction gradient tensor takes an interesting form. In the formation of the WVM for RDT, the particle velocity and wave vector are modeled after the Fourier mode of velocity, $\hat{\boldsymbol{u}}$, and a time evolving unit wave number vector,

$\hat{e}$. The Fourier transform of the fluctuating velocity gradient, $\partial u_i/\partial x_j$, is $\kappa \hat{u}_i \hat{e}_j$, where κ is the magnitude of the wave number vector. The normalized interaction gradient tensor is a tensor representation of the fluctuating velocity gradient and takes a form analogous to its Fourier transform.

The diffusion in the velocity equation is replaced by a statistically equivalent term to achieve a model in a form similar to the general **u-e** decay model. Two stochastic models for the diffusion in the velocity equation are considered

$$dX_i = -\epsilon_{ipq} dW_p e_q^* \tag{17}$$

and

$$dY_i = \left(\delta_{ij} - e_i^* e_j^*\right) dW_j. \tag{18}$$

Each realization of the stochastic increments differ, but the models are statistically equivalent. The conditional mean of the increments are zero while the conditional covariance of the increments are equal,

$$\langle dX_i dX_j | \boldsymbol{e}^* = \eta \rangle = \langle dY_i dY_j | \boldsymbol{e}^* = \eta \rangle = (\delta_{ij} - \eta_i \eta_j). \tag{19}$$

The governing equations for the joint PDF of velocity and wave vector, $f(\boldsymbol{v}, \boldsymbol{\eta}; t)$, are then identical

$$\frac{\partial f}{\partial t} = \frac{1}{2} \frac{\partial^2}{\partial v_i \partial v_j} \left[f \left(\delta_{ij} - \frac{\eta_i \eta_j}{\eta_s \eta_s} \right) \right] + \cdots, \tag{20}$$

where $(\boldsymbol{\eta}, \boldsymbol{v})$ are the state space variables for $(\boldsymbol{e}^*, \boldsymbol{u}^*)$. The IPRM is then modified to

$$\begin{aligned} du_i^* &= -\left(\frac{\varepsilon}{2k}\right) g_{mn} u_n^* \left[\delta_{im} - (2a_e + 1) e_i^* e_m^*\right] dt - \left(\frac{a_u \varepsilon}{k}\right) \hat{\Omega}^* f_{pq} e_p^* e_q^* u_i^* dt \\ &\quad + \left[\left(\frac{a_u \varepsilon}{k}\right) \hat{\Omega}^* f_{pq} e_p^* e_q^* u_s^* u_s^*\right]^{1/2} \left(\delta_{ij} - e_i^* e_j^*\right) dW_j, \end{aligned} \tag{21}$$

which is statistically identical to Eq. (14).

The return-to-isotropy tensor for the IPRM follows from Eq. (21)

$$\begin{aligned} \phi_{ij} &= \underbrace{g_{ik} r_{kj} + g_{jk} r_{ki}}_{\text{production}} - \frac{2}{3} \delta_{ij} - \underbrace{(2a_e + 1) g_{mn} \left[M_{injm} + M_{jnim}\right]}_{\text{rapid redistribution}} \\ &\quad + \underbrace{a_u \hat{\Omega}^* f_{pq} \left[2M_{ijpq} - \delta_{ij} d_{pq} + L_{ijpq}\right]}_{\text{from SRR}}, \end{aligned} \tag{22}$$

where $L_{ijpq} \equiv \langle e_i^* e_j^* e_p^* e_q^* u_s^* u_s^* \rangle / 2k$ is a fourth-order correlation defined in Kassinos and Reynolds [2]. The non-RDT terms are assumed to act as an additional velocity gradient in the IPRM. The resulting model for the return-to-isotropy tensor in Eq. (22) contains "production" and "rapid redistribution" terms due to the additional velocity gradient. The randomization due to the SRR model adds a term to the modeled return-to-isotropy tensor, but in axisymmetric flows this term is zero ($\hat{\Omega}^* = 0.0$).

2.5 Dissipation Model

The PDF models presented still require additional information for closure. In the implementations for homogeneous turbulence, a mean dissipation equation is applied. The standard dissipation model is

$$\frac{d\varepsilon}{dt} = \frac{\varepsilon^2}{k}\left[C_{\varepsilon 1}\frac{P}{\varepsilon} - C_{\varepsilon 2}\right], \tag{23}$$

where P is the production of turbulent kinetic energy. The values of $C_{\varepsilon 1} = 1.5625$ and $C_{\varepsilon 2} = 1.9$ are selected to yield a typical value for $(P/\varepsilon)_\infty = 1.6$. This model is known to be deficient in rotational flows and Kassinos and Reynolds [3] have developed a model with a rotational correction

$$\frac{d\varepsilon}{dt} = \frac{\varepsilon^2}{k}\left[C_{\varepsilon 1}\frac{P}{\varepsilon} - C_{\varepsilon 2}\right] - C_R\varepsilon\sqrt{d_{mn}\Omega_m\Omega_n}, \tag{24}$$

where $\boldsymbol{\Omega}$ is the mean vorticity vector and the parameters $(C_{\varepsilon 1},\ C_{\varepsilon 2},\ C_R) = (1.5,\ 1.833,\ 0.01)$ are defined. Beyond the specification of the parameters, the new model differs from the standard model only in flows with mean rotation. It provides a significant improvement in the results for the difficult case of an elliptical flow. In the Lang and Iso models, an improvement is found for elliptical flows by altering C_R to 0.1. In all other flows, the standard parameter values of the Kassinos and Reynolds dissipation model are used.

2.6 Model Summary

The key ideas from the construction of the models are summarized below.

- **Iso Model**
  1. Basis: isotropic diffusion of the wave vector in Eq. (7)
  2. Return-to-isotropy tensor: linear in b_{ij} and d^a_{ij}, but additional tensors in Eq. (9) have less physical meaning
  3. Decay model constraints: all four constraints met
- **Lang Model**
  1. Basis: a general model for the return-to-isotropy tensor at the Reynolds stress level of closure in Eq. (12)
  2. Velocity equation: Langevin equation with an anisotropic drift term in Eq. (10)
  3. Decay model constraints: all four constraints met
- **IPRM**

1. Basis: interaction between particles modeled as an additional velocity gradient
2. Interacting particle velocity gradient: tensor form in Eq. (15) relates to the Fourier transform of the fluctuating velocity gradient
3. Slow randomization model (SRR)
   - the rotation of the interacting particle gradient adds a randomization in the particle velocity equation
   - cases exist were SRR is identically zero (e.g., axisymmetric flows)
4. Return-to-isotropy tensor: contains production and rapid redistribution from interacting particle velocity gradient as well as a term from the SRR in Eq. (22)
5. Decay model constraints: constraints 1, 2, and 4 are met, while constraint 3 is discussed below

3 Analysis of IPRM

3.1 Particle vs. Cluster Formulation

In the particle formulation of the WVM, the stochastic equations for individual particles are solved via a Monte Carlo technique which is the standard implementation of PDF methods. The approach is applied to homogeneous turbulence in Van Slooten and Pope [1] and is readily extended to inhomogeneous turbulent flows. The inhomogeneous cases of a temporal shear layer and swirling/non-swirling coaxial jets are studied in Van Slooten, Jayesh, and Pope [4] and Van Slooten and Pope [5].

The cluster formulation is developed in Kassinos and Reynolds [2] as an alternative approach to solving the RDT particle equations. A cluster is defined as a group of particles whose wave vectors are identical for *all* time, and a cluster-average of a particle quantity is defined as the expectation of the quantity over the particles in the cluster. The unconditional mean is then calculated by averaging over all of the clusters. The WVM is implemented in the cluster formulation by solving the wave vector and the cluster-averaged Reynolds stress equations via Monte Carlo techniques. If the wave vector equation is deterministic and independent of the cluster-averaged Reynolds stress tensor (e.g., IPRM), then the definition of the cluster may be simplified to a group of particles having the same $\mathbf{e}^*(t_0)$ for *any* specific t_0. The cluster-average is then the expectation conditioned on a particular value of the wave vector at a certain time, $\langle \cdot | \mathbf{e}^*(t_0) = \boldsymbol{\eta}_0; t \rangle$, and the cluster-averaged Reynolds stress equation is deterministic. For models with stochastic wave vector equations, a cluster represents the behavior of the particles following one trajectory in wave vector space. The equation for the cluster-averaged Reynolds stress tensor then contains stochastic terms that correspond to the stochastic terms in the wave vector equation.

In Kassinos and Reynolds [2], the cluster formulation is demonstrated to have better computational properties than the particle formulation, but there are limitations to the cluster approach. Velocity moments other than the Reynolds stresses cannot be determined from the cluster-averaged Reynolds stress tensor. Therefore, the cluster approach is not directly applicable to inhomogeneous turbulence, because terms such as the turbulent transport and scalar flux are no longer handled explicitly by the method. Also, WVM's are in general not closed at the level of the wave vector and cluster-averaged Reynolds stress tensor (e.g., Iso and Lang models).

3.2 Stability of Particle Formulation

Through numerical simulations, it is found that the particle implementation of the IPRM is unstable in homogeneous shear and elliptical streamline flows. This stability issue is studied through an ensemble of N particles with identical initial wave vectors, $\mathbf{e}^{(n)}(0) = \mathbf{e}^0$ for $n = 1, \cdots, N$. The particle wave vectors are identical for all time in the IPRM, and the ensemble represents the particle version of a cluster. The stability of the ensemble is indicative of the stability of the particle formulation since the cluster-averaged Reynolds stress tensor is a Lagrangian representation of the conditional Reynolds stress tensor. An error tensor is defined that characterizes the difference between the ensemble-averaged and cluster-averaged Reynolds stress tensor

$$\lambda_{ij} \equiv \frac{1}{N}\sum_{n=1}^{N} u_i^{(n)} u_j^{(n)} - \langle u_i u_j | \mathbf{e}^0 \rangle, \tag{25}$$

which evolves by

$$\begin{aligned} d\lambda_{ij} \;=\; & -\left(\frac{\varepsilon}{2k}\right)\left[g_{in}\lambda_{nj} + g_{jn}\lambda_{ni}\right] + \left(\frac{\varepsilon}{2k}\right)(2a_e{+}1) g_{mn}\left[e_j^* e_m^* \lambda_{in} + e_i^* e_m^* \lambda_{jn}\right] \\ & -\left(\frac{a_u \varepsilon}{k}\right)\hat{\Omega}^* f_{pq} e_p^* e_q^* \left[2\lambda_{ij} - \left(\delta_{ij} - e_i^* e_j^*\right)\lambda_{ss}\right] \\ & +\left[\left(\frac{a_u \varepsilon}{k}\right)\hat{\Omega}^* f_{pq} e_p^* e_q^*\right]^{1/2} \\ & \times \frac{1}{N}\sum_{n=1}^{N}\left(u_s^{(n)} u_s^{(n)}\right)^{1/2}\left[u_i^{(n)}\left(\delta_{jl} - e_j^* e_l^*\right) + u_j^{(n)}\left(\delta_{il} - e_i^* e_l^*\right)\right] dW_l^{(n)}, \end{aligned} \tag{26}$$

as can be deduced from Eq. (21). Both the limit as $N \to \infty$ and the conditional expectation of the error are zero by definition,

$$\lim_{N\to\infty} \lambda_{ij} = 0 \tag{27}$$

and

$$\langle \lambda_{ij} | \mathbf{e}^0 \rangle = \frac{1}{N}\sum_{n=1}^{N} \langle u_i^{(n)} u_j^{(n)} | \mathbf{e}^0 \rangle - \langle u_i u_j | \mathbf{e}^0 \rangle = 0. \tag{28}$$

The conditional expectation of the second invariant of the error tensor, $I\!I \equiv \langle \lambda_{ij}\lambda_{ij}|\mathbf{e}^0\rangle$ characterizes the magnitude of the error for a finite ensemble and evolves by

$$\begin{aligned}\frac{dI\!I}{dt} &= -\left(\frac{\varepsilon}{k}\right)\left[g_{in}\langle\lambda_{ij}\lambda_{nj}|\mathbf{e}^0\rangle + g_{jn}\langle\lambda_{ij}\lambda_{ni}|\mathbf{e}^0\rangle\right] \\ &+ \left(\frac{\varepsilon}{k}\right)(2a_e+1)g_{mn}\left[e_j^*e_m^*\langle\lambda_{ij}\lambda_{in}|\mathbf{e}^0\rangle + e_i^*e_m^*\langle\lambda_{ij}\lambda_{jn}|\mathbf{e}^0\rangle\right] \\ &- \left(\frac{2a_u\varepsilon}{k}\right)\hat{\Omega}^* f_{pq}e_p^*e_q^*\left[2I\!I - \left(\delta_{ij} - e_i^*e_j^*\right)\langle\lambda_{ij}\lambda_{ss}|\mathbf{e}^0\rangle\right] \\ &+ \left(\frac{6a_u\varepsilon}{k}\right)\hat{\Omega}^* f_{pq}e_p^*e_q^*\frac{\langle(u_su_s)^2|\mathbf{e}^0\rangle}{N}. \end{aligned} \tag{29}$$

The first three terms do not provide a stability problem since the dissipation to kinetic energy ratio does not typically grow without bound, and the error is made small for suitably large N. The final term is proportional to $1/N$, but the expectation $\langle(u_su_s)^2|\mathbf{e}^0\rangle$ is likely to grow exponentially for some values of $\mathbf{e}^0$ in certain flows. In the cases of homogeneous shear and elliptical streamline flows, the particle implementation of the IPRM is found to become unstable after a certain time. This time to blow up is found to increase with the number of particles in the simulation, which is consistent with Eq. (29).

3.3 Return-to-Isotropy Modeling

The Iso and Lang models are based on an assumption that the primary effects of the non-RDT terms is to impose a return-to-isotropy on not only the Reynolds stress tensor, but also the directional spectrum. The isotropic form of the directional spectrum

$$\Gamma_{ij}(\boldsymbol{e}) = \frac{k}{4\pi}(\delta_{ij} - e_ie_j), \tag{30}$$

and the directional energy spectrum

$$\Gamma(\boldsymbol{e}) \equiv \frac{1}{2}\Gamma_{ll}(\boldsymbol{e}) = \frac{k}{4\pi}, \tag{31}$$

are known. The modeled PDF's of velocity from the Iso and Lang models are also designed to decay to a joint normal distribution in isotropic turbulence.

Neither a return-to-isotropy behavior nor a decay to a joint normal distribution of the velocity PDF is explicitly demanded of the IPRM in its construction. A brief analysis is performed on an extreme case that illustrates potential problems in the behavior of the IPRM. A turbulent flow is considered in which the directional and directional energy spectra are non-isotropic and defined by

$$\Gamma_{ij}(\boldsymbol{e}) = (\delta_{ij} - e_ie_j)\Gamma(\boldsymbol{e}) \tag{32}$$

and

$$\Gamma(\boldsymbol{e}) = \frac{k}{4}\sum_{n=1}^{4}\delta(\boldsymbol{e} - \boldsymbol{\eta}^{(n)}), \tag{33}$$

where $\boldsymbol{\eta}^{(n)}$ are four unit vectors in a tetrahedral configuration. The corresponding Reynolds stress and dimensionality tensors are isotropic which gives an isotropic form for the normalized interaction gradient tensor, $g_{mn} = \delta_{mn}$. The particle equations for the IPRM are greatly simplified in this case

$$de_i^* = 0 \tag{34}$$

and

$$du_i^* = -\left(\frac{\varepsilon}{2k}\right) u_i^* dt. \tag{35}$$

The PDF of velocity will not decay to a joint normal distribution without the diffusion term in the Langevin equation for the particle velocity. For the directional spectrum and directional energy spectrum, the governing equations are

$$\frac{d\Gamma_{ij}}{dt} = -\left(\frac{\varepsilon}{k}\right) \Gamma_{ij} \tag{36}$$

and

$$\frac{d\Gamma}{dt} = -\left(\frac{\varepsilon}{k}\right) \Gamma. \tag{37}$$

Both spectra decay in magnitude, but there is no evolution to the isotropic, uniform directional energy spectrum. The fundamental problem is a lack of diffusion in the particle equations for this case.

The wave vector equation in the IPRM contains no diffusion, while the diffusion due to the SRR model in the velocity equation is identically zero in some cases (e.g., axisymmetric turbulence). Without diffusion it is difficult to characterize the return-to-isotropy behavior of the IPRM for general flows. It is suggested that further implementations of the IPRM to decaying turbulence be performed.

4 Applications in Homogeneous Turbulence

The Iso and Lang models and the IPRM are applied to homogeneous turbulence in Van Slooten and Pope [1] and Kassinos and Reynolds [3], respectively. Some of the cases studied in these references include: homogeneous shear with/without frame rotation; axisymmetric contraction and expansion; and elliptical streamline flows. A summary of these results is contained here for the purpose of model comparison.

In the case of homogeneous shear without frame rotation, the simulations are compared to the experimental data of Tavoularis and Karnik [6] and the DNS data of Rogers, Moin, and Reynolds [7]. The Lang model predicts the Reynolds stress anisotropy better than the IPRM, but it may be seen from Table 4 that both models perform quite well. The Iso model, however, fails to correctly distribute the kinetic energy amongst the span-wise and cross-stream normal Reynolds stresses. The predicted kinetic energy evolution for homogeneous shear with frame rotation is compared to the large-eddy simulation data of Bardina, Ferziger, and Reynolds [8].

Table 1: Asymptotic values for homogeneous shear flows from: experiments of Tavoularis and Karnik [6] (TK); DNS data of Rogers, Moin, and Reynolds [7] (RMR); Isotropic Diffusion of e Model (Iso) and Langevin Velocity Model (Lang) wave vector models with Standard (St) and Kassinos and Reynolds (KR) dissipation models; and Interacting Particle Representation Model [3] (IPRM).

	TK	RMR	Lang St	Lang KR	IPRM	Iso St	Iso KR
b_{11}^{∞}	0.18 ± 0.04	0.215	0.194	0.204	0.26	0.223	0.231
b_{12}^{∞}	-0.16 ± 0.01	-0.158	-0.165	-0.167	-0.16	-0.156	-0.156
b_{22}^{∞}	-0.11 ± 0.02	-0.153	-0.131	-0.137	-0.17	-0.203	-0.206
b_{33}^{∞}	-0.06 ± 0.03	-0.062	-0.063	-0.067	-0.08	-0.020	-0.026
$(\mathbf{P}/\varepsilon)_{\infty}$	1.47 ± 0.14	1.80	1.60	1.72	1.86	1.60	1.59
$(Sk/\varepsilon)_{\infty}$	4.60 ± 0.14	5.7	4.83	5.15	5.97	5.12	5.12

All three models provide the correct qualitative behavior (not shown), but the quantitative comparison is poor, a common result among second-order closures.

The comparisons in the cases of axisymmetric contraction and expansion are much more interesting. For axisymmetric contraction, DNS data by Lee and Reynolds [9] exist at various initial normalized strain-rates. The assumptions of RDT apply for the highest strain-rate case $(Sk/\varepsilon)_0 = 55.7$ where $S \equiv \max(\nabla\langle\mathbf{U}\rangle)$. All of the models provide an exact representation of RDT and predict the data in this case very well. In Fig. 1, the Reynolds stress anisotropies from the models are compared to the DNS data for the low strain-rate case, $(Sk/\varepsilon)_0 = 0.557$, and to the experimental data of Tucker [10] with $(Sk/\varepsilon)_0 = 2.1$. The IPRM and Iso models predict the DNS data very well, but both models over-predict the anisotropy from the experimental data. The Lang model predicts the experimental data quite well, but under-predicts the data from the low strain-rate DNS case. The Reynolds stress anisotropy budgets from the models are compared to the low strain-rate DNS data in Fig. 2, where $\mathbf{P}_{ij}^{(b)}/S$, $\mathbf{\Pi}_{ij}^{(r)}/(2kS)$, and $-(\varepsilon/2Sk)\,(\phi_{ij} - 2b_{ij})$ represent the production of anisotropy, the normalized rapid pressure–rate-of-strain correlation, and the return-to-isotropy of the anisotropy, respectively. With the production treated explicitly, the difference in the anisotropies is primarily due to the modeling of the return-to-isotropy tensor. The IPRM and Iso model have a significantly smaller return to isotropy than that of Lang model, which is appropriate for this case. It appears that the small return-to-isotropy is, however, inappropriate for the experimental data.

The modeling of the return-to-isotropy tensor also plays a crucial role in the simulation of axisymmetric expansion. The DNS data of Lee and Reynolds [9] at low and high initial strain-rates, $(Sk/\varepsilon)_0 = 0.408$ and 40.8, are compared to the model predictions of the Reynolds stress anisotropies in Fig. 3. All models match the high strain-rate (i.e., near RDT) case very well, but there is a markedly different

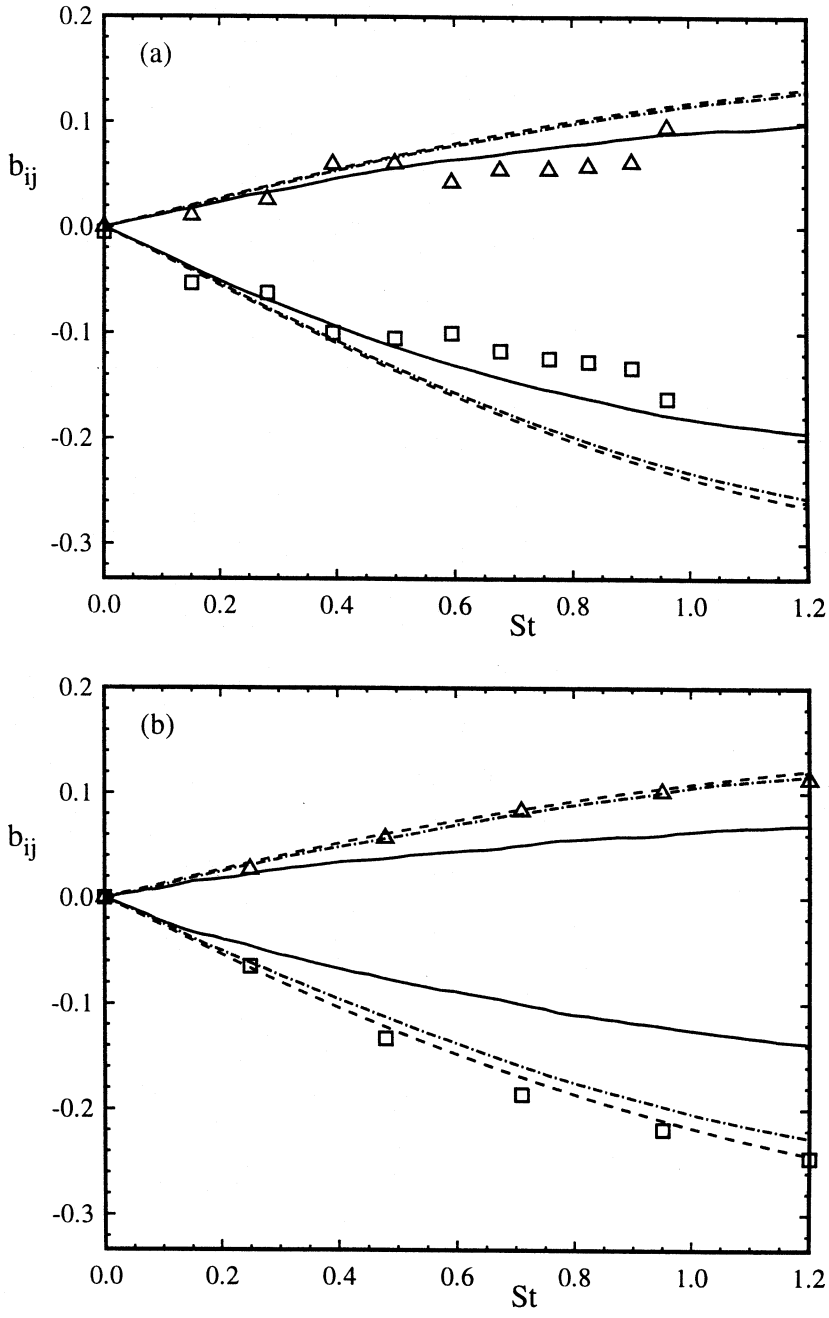

Figure 1: Evolution of Reynolds stress anisotropies in axisymmetric contraction with: —, Lang; ---, IPRM; and -·-, Iso; models compared to: (a) experimental data (Tucker [10]); and (b) DNS data (Lee and Reynolds [9]); where: □, b_{11}; and △, b_{22}.

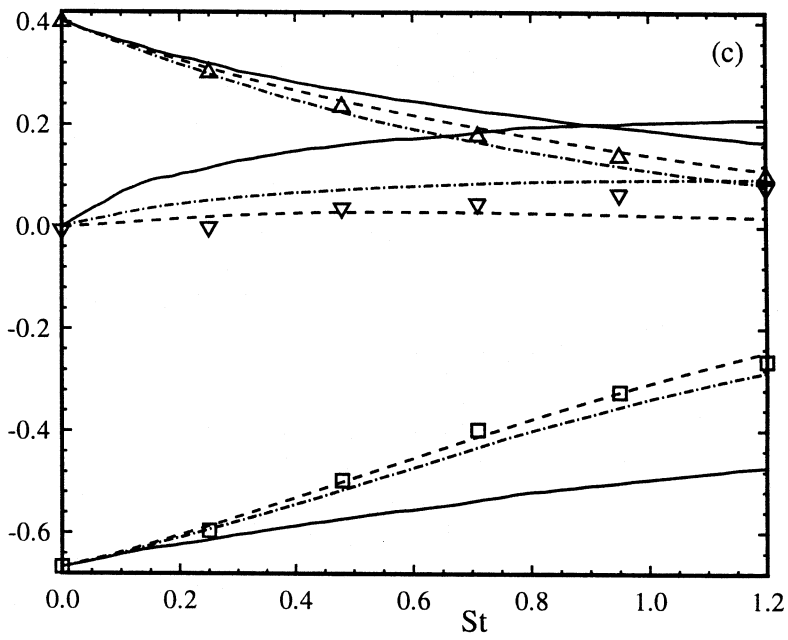

Figure 2: Evolution of Reynolds stress anisotropy budget for the 11-component of axisymmetric contraction with: —, Lang; ---, IPRM; and -·-, Iso; models compared to the DNS data of Lee and Reynolds [9] in the $(Sk/\varepsilon)_0 = 0.557$ case where: $\square$, $\mathbf{P}_{11}^{(b)}/S$; $\triangle$, $\mathbf{\Pi}_{11}^{(r)}/(2kS)$; and ∇, $-(\varepsilon/2Sk)\,(\phi_{11} - 2b_{11})$.

behavior between the models in the low strain-rate case. The IPRM predicts an increased anisotropy as in the DNS data, while the Iso and Lang models predict a decrease of the anisotropy. An examination of the anisotropy budgets in Fig. 4 shows that the source of the difference is again the return-to-isotropy model. The return-to-isotropy of the anisotropy term consists of two parts: the return-to-isotropy tensor and a normalization term, $(\varepsilon/Sk)b_{ij}$. For the DNS data and the IPRM, the return-to-isotropy tensor is smaller than the normalization term, and the return-to-isotropy of the anisotropy actually increases the anisotropy of the flow! This behavior is not captured by any standard Reynolds stress model.

The final case considered is the elliptic streamline flow for which DNS data is reported in Blaisdell and Shariff [11] and [12]. Elliptical streamlines are generated by the mean velocity gradient:

$$\frac{\partial \langle U_i \rangle}{\partial x_j} = \begin{bmatrix} 0 & 0 & S+\omega \\ 0 & 0 & 0 \\ S-\omega & 0 & 0 \end{bmatrix}, \tag{38}$$

with $|\omega| > |S|$, while $|\omega| < |S|$ generates hyperbolic streamlines. The flow is parameterized by the aspect ratio of the elliptical streamlines, $E \equiv \sqrt{(S+\omega)/(\omega - S)}$, and the initial Rossby number, $R_0 \equiv (\varepsilon/k\omega)_0$, where $\Omega \equiv \sqrt{(S+\omega)(\omega - S)}$ is the rotational frequency. The case e2 from Blaisdell and Shariff [12] is selected in which $E = 1.25$, $\Omega = 4.44$, and $R_0 = 0.133$. Model results are only shown for the Lang and Iso models, because the particle simulation of the IPRM is numerically unstable for elliptical flows (see Sec. 3.2). Both a stability analysis and the DNS data indicate that the kinetic energy grows exponentially in this case. From Fig. 5, the Lang and Iso models predict an exponential growth, but do not capture the correct rate. In Fig. 6, the anisotropies of the normal Reynolds stresses are predicted quite well by the Iso and Lang models, but both models severely under-predict the anisotropy of the shear stress. From the results in Kassinos and Reynolds [3], the IPRM appears to capture better the growth of the shear stress indicated by the DNS data. The RDT solution is also shown in Figs. 5 and 6, and provides surprisingly good comparisons with the DNS data for the anisotropies. However, the kinetic energy grows too rapidly without any dissipation, and the oscillations do not decay as in the DNS data.

The fact that the RDT solution compares favorably with the DNS data is an indication that the turbulent cascade process may not be fully developed. The cascade process is represented in the Reynolds stress equation by the dissipation and the return-to-isotropy tensor and is known to be strongly affected by both rotation and Reynolds number. The dissipation is the loss of kinetic energy at the large scales due to the cascade of energy to the small scales, and corrections to the modeled dissipation equation are often required for rotating flows (e.g., Sec. 2.5). A decreasing Reynolds number alters the cascade process through a decrease in the separation of the dissipative and energetic scales. The slow pressure–rate-of-strain correlation in the return-to-isotropy tensor acts to scramble the Reynolds stresses

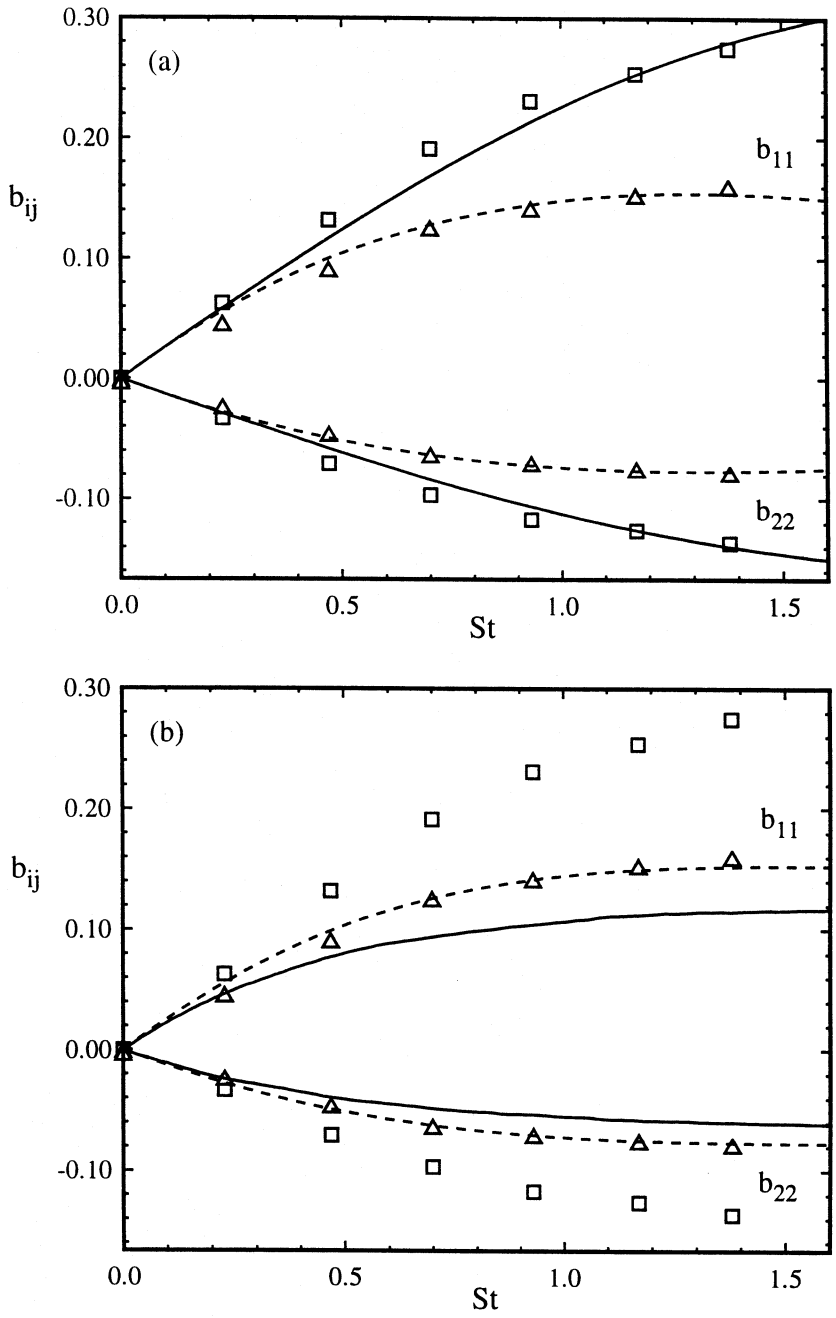

Figure 3: Evolution of Reynolds stress anisotropies in axisymmetric expansion from: (a) IPRM; (b) Iso model; and (c) Lang model; compared to the DNS Data of Lee and Reynolds [9] (symbols) for: (—, □), $(Sk/\varepsilon)_0 = 0.408$; and (---, △), $(Sk/\varepsilon)_0 = 40.8$.

Figure 3 (Continued)

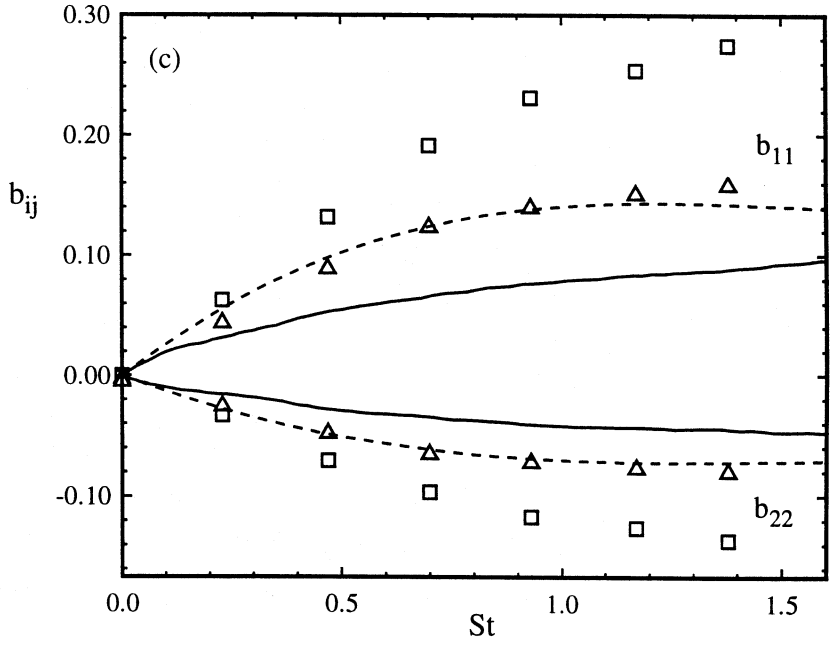

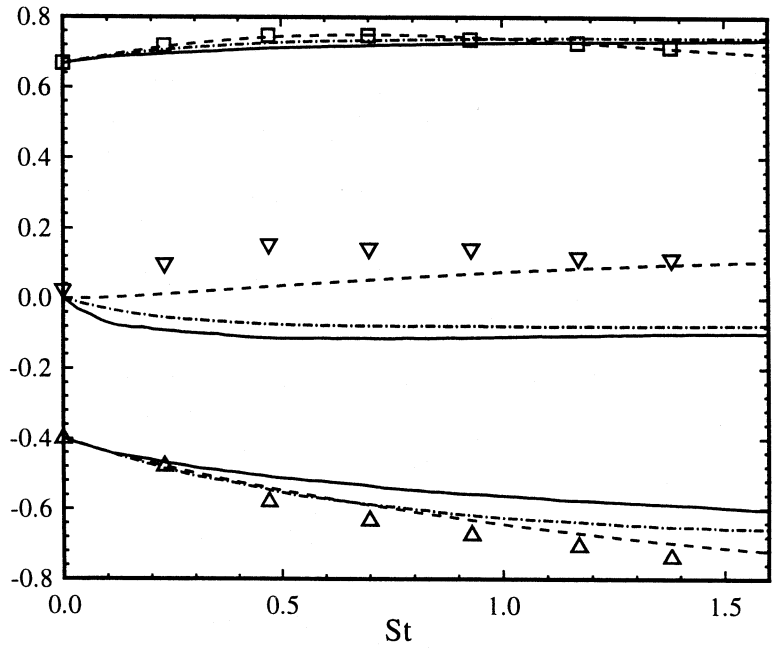

Figure 4: Evolution of Reynolds stress anisotropy budget for the 11-component of axisymmetric expansion with: —, Lang; ---, IPRM; and -·-, Iso; models compared to the DNS data of Lee and Reynolds [9] in the $(Sk/\varepsilon)_0 = 0.408$ case where: □, $\mathbf{P}_{11}^{(b)}/S$; △, $\mathbf{\Pi}_{11}^{(r)}/(2kS)$; and ∇, $-(\varepsilon/2Sk)\,(\phi_{11} - 2b_{11})$.

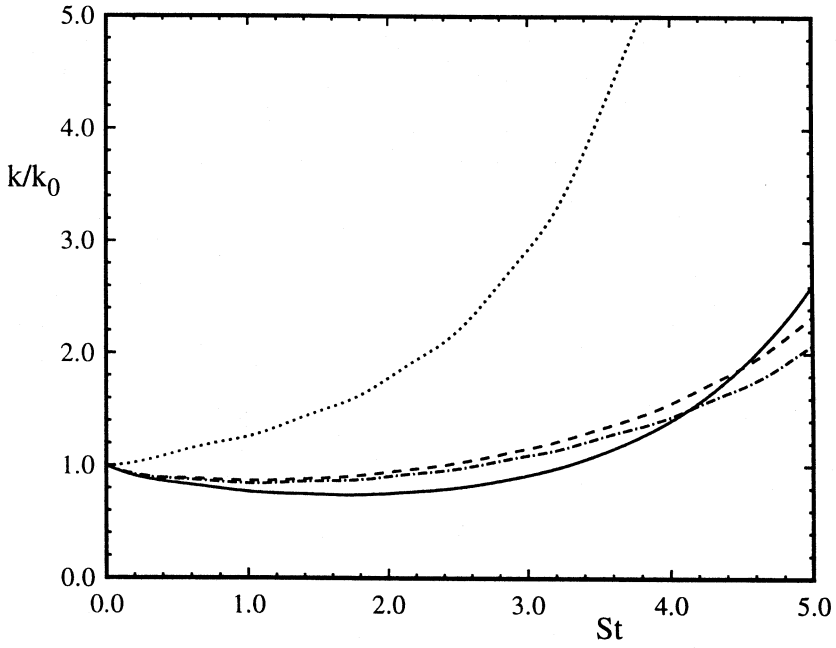

Figure 5: Evolution of kinetic energy in elliptical streamline flow with $E = 1.25$ and $R_0 = 0.133$ for: —, DNS of Blaisdell and Shariff [11]; ---, Lang; -·-, Iso; and $\cdots$, RDT.

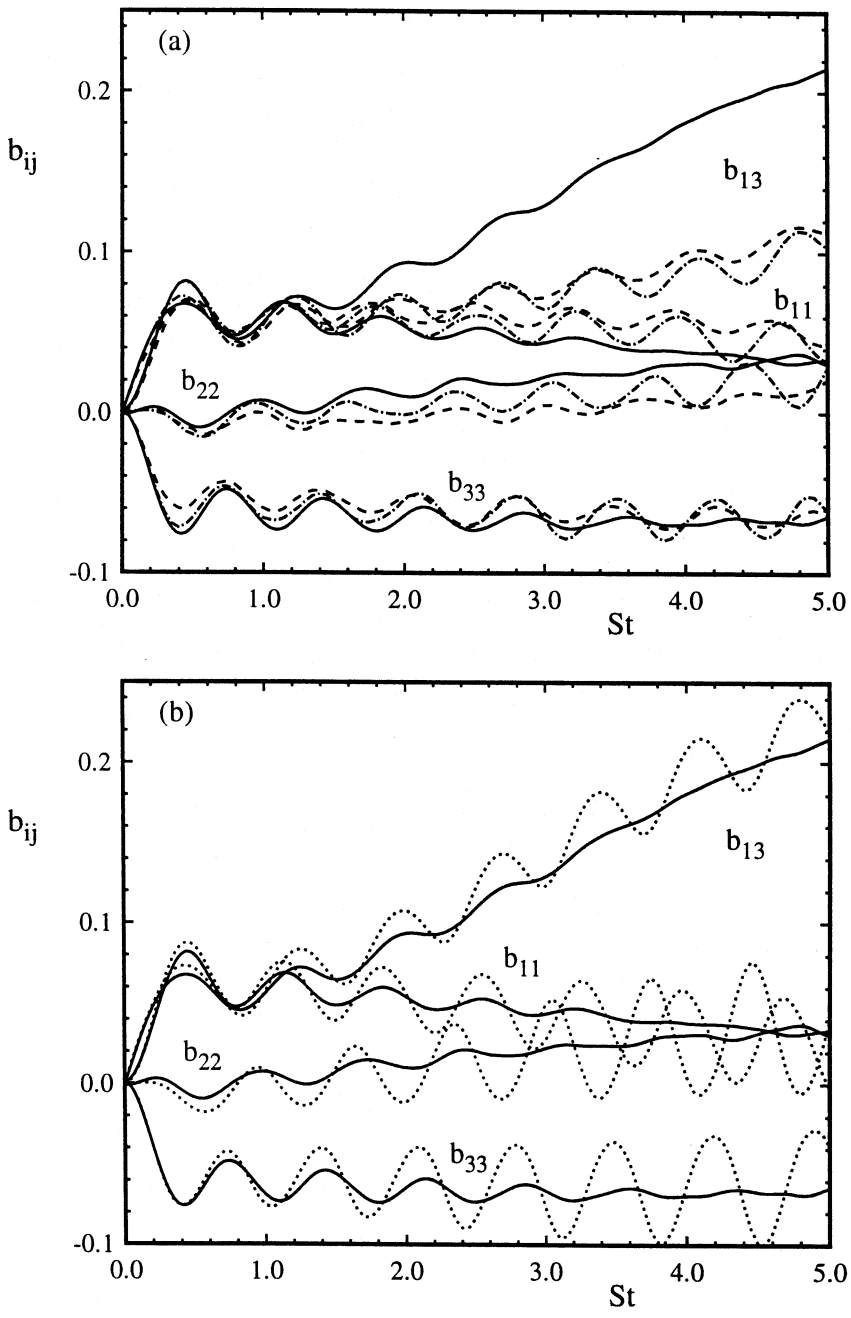

Figure 6: Evolution of Reynolds stress anisotropies in an elliptical streamline flow with $E = 1.25$ and $R_0 = 0.133$ for (a): —, DNS of Blaisdell and Shariff [11]; ---, Lang; and -·-, Iso; and for (b): —, DNS of Blaisdell and Shariff [11]; and · · ·, RDT.

Table 2: Turbulent Reynolds number of DNS data from: Rogers, Moin, and Reynolds [7] (RMR); Lee and Reynolds [9] (LR); and Blaisdell and Shariff [12] (BS) in homogeneous shear (HS), axisymmetric contraction (AXC) and expansion (AXE), and elliptical streamline flow (ELL).

Reference	Case	$R_t \equiv 4k^2/\varepsilon\nu$
RMR	HS	$150 \sim 1500$
LR	AXC	$48 \sim 61$
LR	AXE	$44 \sim 88$
BS	ELL	51

and is strongly Reynolds number dependent.

The IPRM provides good predictions of the DNS data in an elliptical streamline flow and axisymmetric contraction and expansion. There is relatively little return-to-isotropy in these cases which is modeled correctly by the IPRM. The Iso and Lang models have a greater return-to-isotropy and fail to correctly represent some of these cases. However, the Lang model provides better predictions than either the IPRM or Iso model in an experimental case of axisymmetric contraction and in homogeneous shear. The return-to-isotropy tensor in decaying turbulence is known to have a dependence on the Reynolds number of the flow, and numerous researchers have developed models with a strong Reynolds number dependency (e.g., Lumley and Newman [13] and Chung and Kim [14]). The turbulent Reynolds numbers, $R_t \equiv 4k^2/\nu\varepsilon$, for the DNS data previously examined are provided in Table 4 and are quite low in all but the homogeneous shear case. For inhomogeneous turbulence at high Reynolds numbers, the return-to-isotropy tensor can be an important term. As an example, it is the dominant source of cross-stream normal stress in a temporal shear layer. Therefore, it is reasonable to be concerned about the application of the IPRM to high Reynolds number flows, despite its very good performance in the cases illustrated here.

5 Summary and Conclusions

The important observations developed in this work follow.

1. The Iso model in Eqs. (7) and (8) and the Lang model in Eqs. (10) and (11) are coupled stochastic differential equations (SDE's) for the velocity and wave vector.

2. The IPRM consists of an ordinary differential equation (ODE) for the wave vector in Eq. (13) and an SDE for the velocity in Eq. (14) or equivalently in Eq. (21). For a specific class of flows where $\hat{\Omega}^*$ is zero the velocity equation becomes an ODE.

3. In the rapid distortion limit, all models simplify to the WVM for RDT, Eqs. (1) and (2), which is an exact representation of the flow.

4. In the absence of mean velocity gradients, the Iso and Lang models meet all four constraints of a decay model, while the IPRM in general does not cause the PDF of velocity to tend to an isotropic joint-normal distribution.

5. In the Lang model, the return-to-isotropy tensor in Eq. (12) is a general function of the Reynolds stress anisotropy, while in the Iso model, Eq. (9), the tensor is modeled as a linear function of the Reynolds stress and dimensionality anisotropies with additional terms. For the IPRM, the return-to-isotropy tensor in Eq. (22) contains a production and rapid redistribution of the interacting particle gradient as well as a term from the SRR. Further applications to decaying turbulence are required to characterize the behavior of the IPRM's return-to-isotropy tensor.

6. The cluster formulation improves the numerical implementation of the WVM's, but is not directly applicable to all models nor to inhomogeneous turbulence. The particle formulation is appropriate for inhomogeneous turbulence, but the particle implementation for the IPRM is unstable in some flows.

7. The IPRM provides very good results in comparison with DNS data even for the difficult case of elliptical streamline flows. However, the DNS data is at low Reynolds numbers where the return-to-isotropy is weak.

8. The addition of new stochastic terms to the IPRM that are possibly Reynolds number dependent may prove worthwhile for high Reynolds number flows and may also improve the stability of the IPRM's particle implementation.

9. The Iso model performs worse than both the IPRM and Lang model for the important case of homogeneous shear and is not recommended for further study.

10. The Lang model performs well in homogeneous shear and in several cases of inhomogeneous turbulence (the temporal shear layer and swirling/non-swirling co-axial jets). In comparison with some low Reynolds number DNS data, the Lang model provides a too strong return-to-isotropy.

11. More sophisticated RSM's can be represented through the Lang model by changing the constant coefficients into functions of the Reynolds number and anisotropy invariants.

References

[1] P. R. Van Slooten and S. B. Pope. PDF modeling for inhomogeneous turbulence with exact representation of rapid distortions. *Phys. Fluids*, 9(4):1085, 1997.

[2] S.C. Kassinos and W.C. Reynolds. A structure-based model for the rapid distortion of homogeneous turbulence. Technical Report TF-61, Stanford University, 1994.

[3] S. C. Kassinos and W. C. Reynolds. A particle representation model for the deformation of homogeneous turbulence. *Annual Research Briefs: Center for Turbulence Research*, page 31, 1996.

[4] P. R. Van Slooten, Jayesh, and S. B. Pope. Advances in PDF modeling for inhomogeneous turbulent flows. *Phys. Fluids*, 10(1), 1998. (accepted).

[5] P. R. Van Slooten and S. B. Pope. Application of PDF modeling to swirling and non-swirling turbulent jets. (to be submitted), 1997.

[6] S. Tavoularis and U. Karnik. Further experiments on the evolution of turbulent stresses and scales in uniformly sheared turbulence. *J. Fluid Mech.*, 204:457, 1989.

[7] M. M. Rogers, P. Moin, and W. C. Reynolds. The structure and modeling of the hydrodynamic and passive scalar fields in homogeneous turbulent shear flow. Technical Report TF-25, Stanford University, 1986.

[8] J. Bardina, J. H. Ferziger, and W. C. Reynolds. Improved turbulence models based on large-eddy simulation of homogeneous, incompressible turbulent flows. Technical Report TF-19, Stanford University, 1983.

[9] M. J. Lee and W. C. Reynolds. Numerical experiments on the structure of homogeneous turbulence. Technical Report TF-24, Stanford University, 1985.

[10] H. J. Tucker. PhD thesis, McGill University, 1970.

[11] G. A. Blaisdell and K. Shariff. Homogeneous turbulence subjected to mean flow with elliptic stream lines. In *Studying Turbulence Using Numerical Simulation Databases - V*, December 1994. Center for Turbulence Research: Proceedings of the Summer Program 1994.

[12] G. A. Blaisdell and K. Shariff. Simulation and modeling of the elliptic streamline flow. In *Center for Turbulence Research: Proceedings of the Summer Program 1996*, 1996.

[13] J. L. Lumley and G. R. Newman. The return to isotropy of homogeneous turbulence. *J. Fluid Mech.*, 82:161–178, 1977.

[14] M. K. Chung and S. K. Kim. A nonlinear return-to-isotropy model with Reynolds number and anisotropy dependency. *Phys. Fluids*, 7(6):1425, June 1995.